Bidirectionally injection-locked coupled microring GaN lasers

Shinji Tohi,[1,2] Gal Harari,[3] Takumi Ito,[2] Yaakov Lumer,[3] Miguel A. Bandres,[4] Kunimichi Omae,[2] and Mordechai Segev[1,3,*]

[1] *Solid State Institute, Technion – Israel Institute of Technology, Haifa 32000, Israel*
[2] *Research and Development Department, Nichia Corporation, 491 Kaminaka-Oka, Anan, Tokushima, Japan*
[3] *Physics Department, Technion – Israel Institute of Technology, Haifa 32000, Israel*
[4] *CREOL, The College of Optics and Photonics, University of Central Florida, Orlando, Florida 32816, USA*

(Received 30 September 2023; revised 23 December 2023; accepted 16 January 2024; published 7 February 2024)

Coherent high-quality laser sources are important for a variety of photonic devices and applications, yet they are especially challenging for high-power semiconductor lasers, because high-power and single-mode lasing present con icting requirements; high power drives nonlinear processes causing multimode lasing and instabilities. Here, we present a distributed feedback (DFB) microring laser coupled to a uniform ring, which displays single-mode lasing up to 10 times the threshold value. This is the rst microring DFB laser in gallium nitride (GaN) and the rst monolithic coupled microring GaN lasers. Our work paves the way for future designs of high-quality high-power coupled lasers for applications, such as topological lasers, high-power monolithic frequency combs, optical clocks, gyros, sensing, and quantum systems.

DOI: 10.1103/PhysRevApplied.21.024014

I. INTRODUCTION

Microring resonators, both passive and active (lasers), are growing in importance as a key component for optical integrated circuit platforms [1,2]. Speci cally, recently developed fabrication processes are able to achieve ultrahigh-quality-factor (UHQ) resonators with Q factors in the range of $10^7 - 10^8$ [3 7]. These UHQ resonators open a way for a new domain of applications thanks to their increased ability to store high light intensities with a low-power input source, and to store light for a long duration, thus enhancing the e ciency of sensing and nonlinear e ects. These devices have been proposed and demonstrated to generate compact frequency combs [8,9], atomic clocks [10], quantum sensors and qubits [11,12], ultranarrow-linewidth lasers [6,13,14], optical gyroscopes [14 17], and many more applications.

To construct a UHQ resonator, one must minimize the losses in the resonator. This is usually achieved by decreasing the optical losses through surface treatment, and by reducing the bending losses by increasing the resonator s size. This comes at a price: the increased size makes these resonators support many longitudinal modes. For active systems, such as lasers, this is a major caveat as it sets a very tight trade-o between single-mode lasing and high-power lasing.

Here, we propose and demonstrate a system based on coupled microring lasers that o ers an active scalable on-chip system for UHQ applications. Our system consists of a distributed feedback (DFB) microring laser that provides a highly coherent seed, monolithically coupled to an ordinary (smooth waveguide) multimode high-Q-factor microring laser. We speci cally demonstrate experimentally our system in GaN, which lases in the blue and violet frequency regimes. Our results show that the coupled system maintains single-mode lasing up to 10 times the threshold pumping, exceeding the performance of the stand-alone DFB microring, which turns multimode at 4 times the threshold. The key feature that leads to the superior result we present is the fact that the two coupled rings are bidirectionally injection locking each other [18].

The ordinary ring, which normally displays multimode lasing, is forced into single-mode lasing by coupling to the DFB ring laser, and injection locks the DFB laser, thereby enhancing the single-mode lasing of the entire coupled system high above threshold. This work is the rst demonstration of a monolithic coupled microring laser system in GaN. Our system o ers a scheme for scaling up with multiple emitters coupled to the DFB laser, yielding a chip-scale coherent high-power light source in the blue wavelength region emitted from a chip. Thus, our system could be used as the building block in constructing topological insulator laser arrays [19 25]. Using a DFB in arrays of semiconductor lasers would yield an additional asset, by locking all the emitters into the single frequency of the DFB laser. In topological insulator laser arrays, the topological edge mode is immune to defects and disorder caused in the fabrication process, and is not a ected by scaling up the system

*msegev@technion.ac.il

to a large number of lasers simultaneously emitting high-power coherent light. Thus, the work presented here serves as the building block of a future topological array of GaN lasers.

II. EXPERIMENTS

A. DFB microring lasers

Consider first the microring DFB laser. To achieve single-mode lasing in microring lasers, one can introduce a periodic perturbation in the refractive index (or in the gain) along the ring waveguide as in conventional edge-emitting DFB lasers [26,27]. We employ the method demonstrated in GaAs-based microring lasers by Arbabi *et al.* [27]: the periodic grating is engraved on the inner sidewall of the waveguide as shown in Fig. 1(a). Note that, in our system, a second-order grating with a large pitch is implemented to accurately transfer the grating pattern to the waveguide. Furthermore, the second-order DFB laser exhibits two modes, which correspond to the band-edge modes in a one-dimensional photonic crystal (formed due to the periodic refractive index modulation). One of these modes is supported by the grating as a lasing mode, while the other is suppressed due to its higher radiation loss. Thus, intrinsically, the ring with the second-order DFB exhibits single-mode lasing. In our samples, a waveguide of 600-nm width is modulated sinusoidally with an amplitude of 120 nm. The coupling coefficient (κ) of the Bragg reflection in this structure is estimated as 39.2 cm^{-1} by a finite-element method utilizing COMSOL Multiphysics.

The GaN-based epitaxial structure, composed of GaN, (In,Ga)N, and (Al,Ga)N layers, as shown in Fig. 1(b), is grown on the freestanding GaN bulk substrate by metalorganic chemical vapor deposition (MOCVD). To pattern the ring structure, a SiO_2 thin film is deposited by MOCVD on top of the GaN epitaxial layers, and then an electron beam resist (ma-N 2400) is coated on top. The ring pattern is imprinted using electron beam lithography and transferred onto the SiO_2 film (which serves as a hard mask) and GaN structure by using reactive ion etching with CHF_3-O_2 and Cl_2-$SiCl_4$ gas, respectively. To enhance the coupling between the light localized at the active layer and the grating structure, the GaN epitaxial structure is etched down to the *n*-side cladding layer. The photoluminescence spectra of the fabricated samples are shown in Figs. 1(c) and 1(d). Without any grating, the microring laser displays at least five longitudinal modes [see, for example, the spectrum shown in Fig. 1(c)]. Introducing the proper gratings changes the lasing spectrum dramatically: as shown in Fig. 1(c), the microring laser displays a single lasing mode, and the lasing wavelength is selected by the grating period. Note that introducing the highly selective grating may shift the lasing wavelength considerably, as shown in Figs. 1(c) and 1(d). Note that the single-mode suppression ratio for our DFB microring laser is 22 dB. This is because the spontaneous emissions and lasing emissions are collected simultaneously in our system, and the other suppressed longitudinal modes are no longer observable, as they are buried in the spontaneous emission.

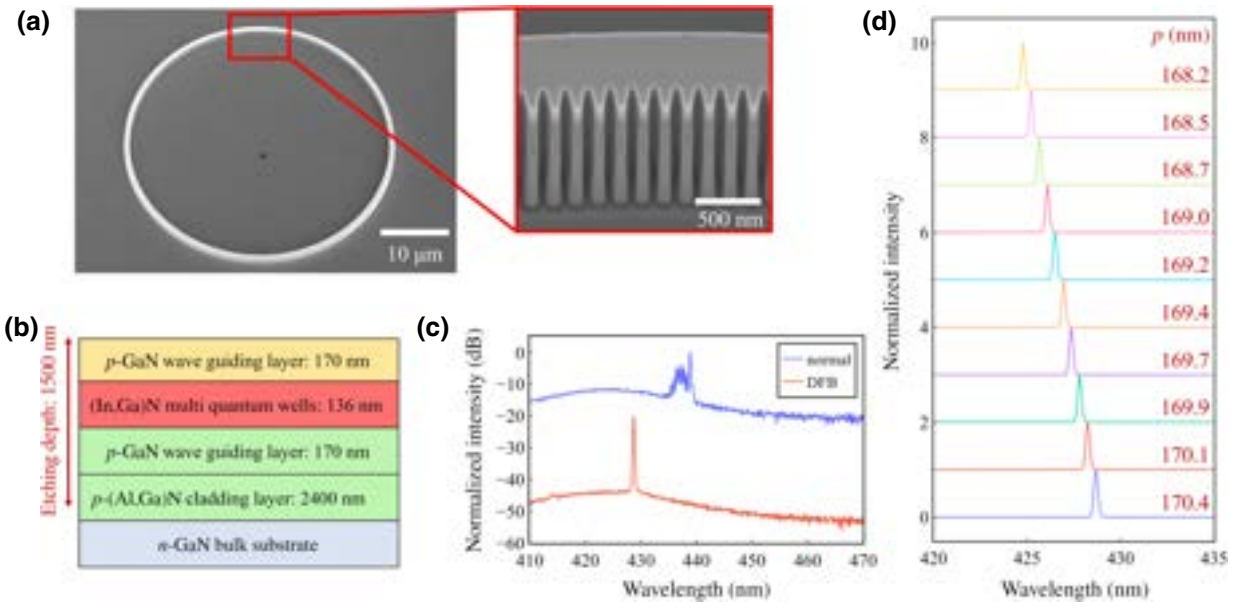

FIG. 1. (a) Scanning electron microscopy images of the DFB ring laser. (b) Epitaxial structure of the GaN microring lasers. (c) Typical lasing spectrum of the ordinary microring laser without grating and the DFB microring laser. Our microring laser has eight longitudinal modes due to the large size of the ring. (d) Controlling the lasing spectra of various DFB ring lasers with various grating periods *p*.

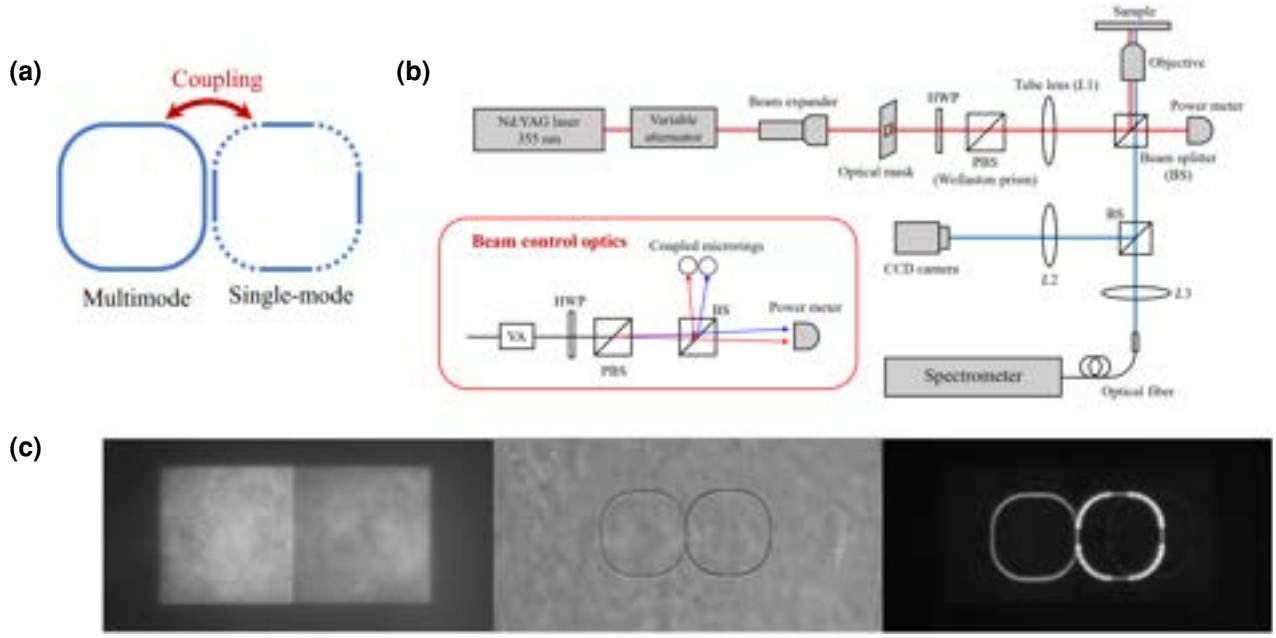

FIG. 2. (a) Schematics of the coupled microring system. Dashed lines represent the grating integrated in the microring waveguides. (b) Measurement setup. Red lines indicate the pump beam and blue lines indicate the propagation of the light emitted from the coupled system. The optics for controlling the pump intensity for coupled rings is shown in the inset. (c) Optical microscope images of the pump beam (left) and coupled microrings without (middle) and with (right) the pump beam.

B. Coupled microring lasers

Next, we construct the coupled microring system. We fabricate two coupled microring lasers: one with a grating and the other without. Figure 2(a) shows the schematics of the coupled microring system comprised of the multimode (left) and the single-mode DFB (right) lasers. Owing to the short lasing wavelength in GaN-based semiconductor lasers and the strong con nement of the light, we nd that the coupling is weak. Consequently, we fabricate racetrack-shaped waveguides, with long parallel regions to get signi cant coupling between the structures. However, in a racetrack resonator, we do not fabricate a grating all around the cavity, since it is di cult to precisely match the operating wavelength between the straight and curved sections of the waveguide due to the di erence in the e ective index. We therefore fabricate the gratings in the four curved sections of the racetrack waveguide, as shown in Fig. 2(a). This allows the coupling strength to be controlled by adjusting the coupling length (the straight regions of the racetracks) and the separation between microrings (around 30 nm). Moreover, if the gratings were introduced in the straight sections, opposing gratings would be optically coupled, causing undesired re ections that could lead to multimode lasing.

We experimentally evaluate the performance of our coupled system in terms of lasing spectrum and power. We measure the lasing spectra while controlling the pumping intensities of the two rings individually as illustrated in Fig. 2(b). The pump laser is a Nd:YAG laser with an operating wavelength of 355 nm, a pulse width of less than 15 ns, and a repetition rate of 10 kHz. The pump beam is structured as a square-like beam of 75 μm per side with a uniform intensity pro le. This is done by the beam-shaping optics consisting of a beam expander and an optical mask. The control over the intensities of the pump beams is achieved by splitting the pump beam using a polarizing beam splitter (PBS) into two beams, one horizontally polarized and the other vertically polarized, and each is set to illuminate a di erent ring. Two branches of the beam are slightly overlapped to prevent an unpumped region. The resulting beam pro les and coupled microring system are shown in Fig. 2(c). In the microscope image in the middle of Fig. 2(c), the normal ring and the DFB ring are indistinguishable, but when the rings are pumped, as in the left of Fig. 2(c), the two become distinguishable because light is strongly scattered upwards in the DFB ring due to fabrication imperfections in the grating. The beam-splitting ratio can be adjusted continuously by rotating the polarization with a half-wavelength plate (HWP) before the PBS, and in combination with a variable attenuator (VA), the pump intensity for the two rings can be controlled independently [see inset in Fig. 2(b)]. The emission from the sample is collected by the objective, imaged onto a charge-coupled device (CCD) camera, and focused onto the optical ber connected to a spectrometer.

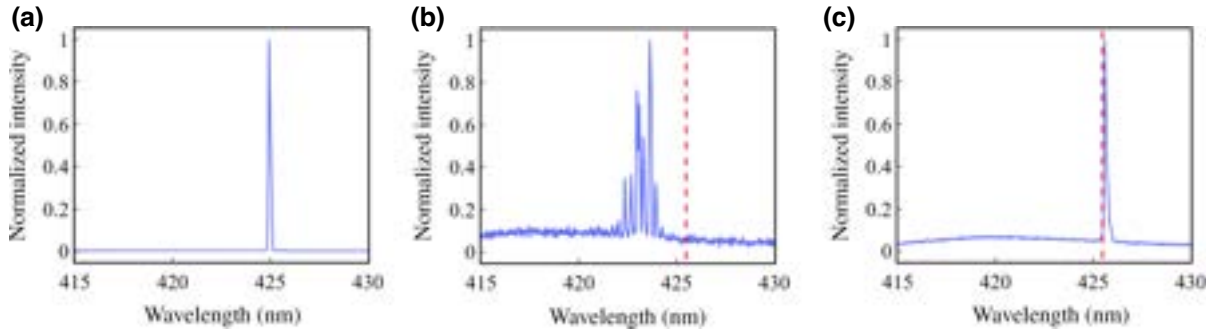

FIG. 3. Typical lasing spectra for (a) a single DFB ring, (b) a free-running uniform multimode ring, and (c) our system consisting of the DFB ring and a uniform ring. The dashed lines indicate the peak wavelength of the single DFB ring. The lasing wavelength of our coupled system is almost the same as the single DFB ring (dashed red line), with a very slight difference within fabrication tolerances.

We pump the two rings at various intensities, up to 3–4 times above the lasing threshold (the maximum pumping intensity depends on the damage threshold of each sample), measure the emitted power and the lasing spectra, and count the number of peaks in the lasing spectra. Figures 3(a)–(c) show an example of the spectrum of a DFB laser, a free-running uniform ring, and the spectrum emitted by the coupled microrings, respectively. Note that the coupling of the DFB to the uniform ring not only yields single-mode lasing [Fig. 3(c)], but also shifts the spectrum of the uniform ring [Fig. 3(b)] from being centered around 423 nm to the wavelength selected by the grating.

Subsequently, to obtain a deeper analysis of the coupled microring system, we map the single- and multimode lasing states for various pumping intensities of the left and right rings. Here, we compare various coupled microring systems with the same free spectral range (same cavity length) but with different coupling strengths (different spacing between rings), in order to evaluate the single-mode nature of the systems, i.e., to make a fair comparison between the lasing mode and the suppression of all other modes. The results for coupled microring lasers with different spacings between the two rings are shown in Fig. 4.

In the sample with the spacing of 500 nm, the two rings are far apart and do not interact with each other. Since the uniform ring is not coupled to the DFB ring, it exhibits a multimode spectrum when pumped above the threshold. On the other hand, the DFB ring exhibits single-mode lasing, but once the uniform ring is also pumped above the threshold, the spectra of the emission from both rings (monitored simultaneously) are multimode. In other words, a single-mode spectrum can be observed only in the region where the pump intensity of the uniform ring is below the threshold [the region on the left of the dashed line in Fig. 4(a)]. When the rings are fabricated at closer proximity such that they are evanescently coupled, the spectrum changes dramatically. Specifically, in the sample with the spacing of 40 nm, we observe single-mode lasing emitted from the coupled rings when pumped above the threshold level of the uniform ring. This indicates that the uniform ring is put into the lasing mode of the DFB ring due to injection locking, and this enhances the single-mode operation due to the bidirectionality of the locking. The overall power emitted from the system is increased by the additional power arising from the uniform ring, while the beam quality of the DFB ring is maintained. Moreover, in the case where the rings are fabricated to be even closer (30 nm), the region of single-mode lasing is further expanded. Thus, by increasing the coupling strength, one can achieve an even greater effect, since the single-mode lasing is maintained even when the ordinary ring is pumped to a considerably higher output power.

Finally, the samples are characterized in the higher power range further above the threshold. Figures 4(d) and 4(e) show the lasing characteristics of the single DFB laser and the coupled microring configuration (both rings are evenly pumped), in terms of intensity and number of the lasing modes. In these experiments, we restrict the pumping ratio to each ring to 50:50, because prolonged exposure by a high-power pump beam degrades the samples. Comparing the two systems, the coupled system can provide single-mode lasing at output power levels 3.8 times higher than the single DFB. Interestingly, we find that, in this regime of coupling, when the DFB is pumped much more strongly than the uniform ring [left side of Fig. 4(c)], the coupled system has two modes. When the uniform ring is pumped more strongly, the coupled system emits a single mode and remains single-mode up to 10 times above the threshold [Fig. 4(e)].

In examining the lasing spectrum of our coupled system, we also notice that the shape of the blank region, where both rings are not lasing, changes significantly when we vary the coupling strength between the rings [in Figs. 4(b) and 4(c)]. This is due to the effect of an exceptional point singularity which changes the lasing threshold of the entire

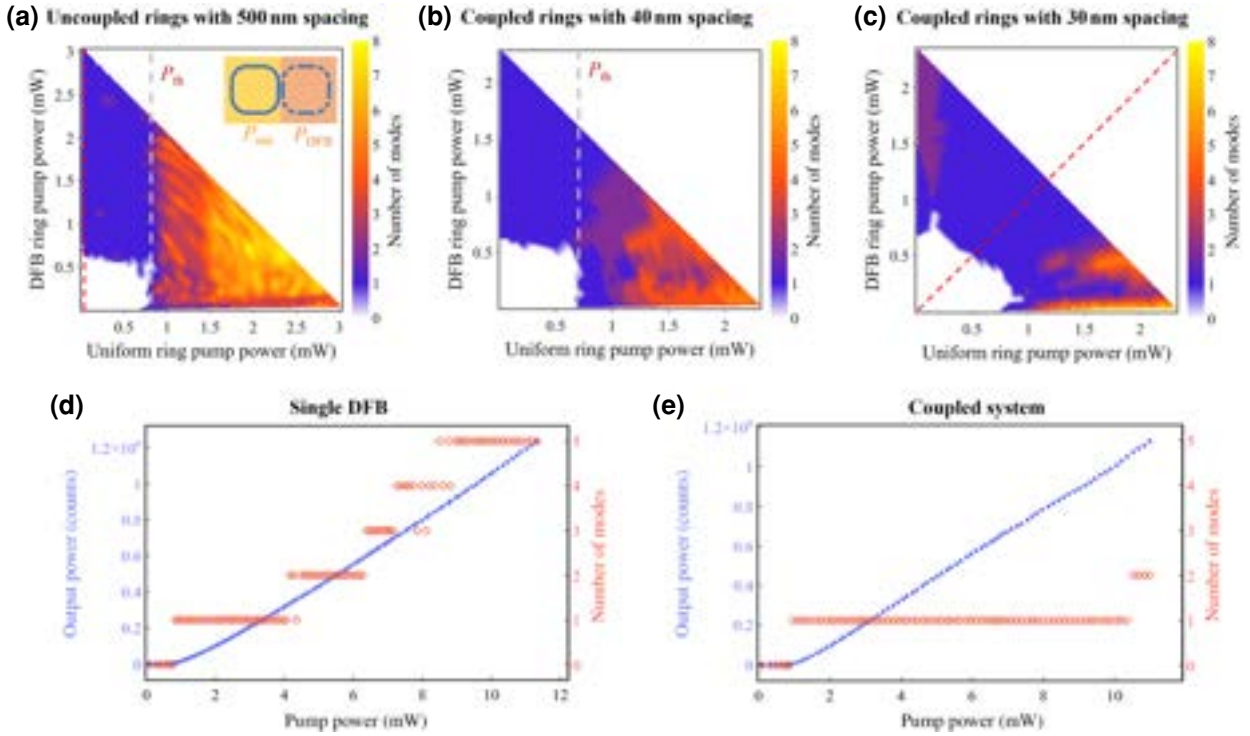

FIG. 4. (a) (c) Number of lasing modes as a function of pumping intensities of the ordinary uniform ring (P_{uni}) and the DFB ring (P_{DFB}). The measurements are performed for samples with the spacing between rings of (a) 500 nm, (b) 40 nm, and (c) 30 nm. Gray dashed lines indicate the lasing threshold of the uniform ring. The upper right inset of (a) shows what takes place in the measurement while pumping at various powers for each ring. (d),(e) Output power and number of lasing modes versus pump power for (d) the single DFB ring and (e) the coupled system. The plots of the number of modes in (d),(e) correspond to the cross-sectional views of the color map sliced by the red dashed lines in (a),(c), respectively. The lasing thresholds (P_{th}) of the single DFB and the coupled system are similar at 0.76 and 0.97 mW, respectively.

system when the gain contrast between the two rings is large [28,29].

III. CONCLUSION

In conclusion, we demonstrate a monolithic semiconductor coupled microring system in GaN. We show that, by employing the single-mode DFB laser as a seed source and coupling it to a multimode uniform ring laser, the output from the entire system is similar to the sum of the power emitted from the DFB and the uniform ring when pumped individually, while single-mode lasing is maintained. The stability of the single-mode lasing is ensured by injection locking that forces the entire system into the DFB mode. Our work paves the way to large-scale ring laser arrays with a large ampli cation e ect, for example, by using a topological insulator laser scheme [18 24] to further extend the robustness of the system. Moreover, this method could also be used in high-Q applications such as high-power sensors (gyros, magnetic elds, time, frequency, etc.), frequency combs, and narrow-linewidth high-power platforms. One of the challenges for the future is to develop practical devices, which would have to be electrically pumped. In GaN-based systems, current-injection microdisk lasers have already been demonstrated [30 32], hence we expect that our system can be transitioned to a current-injection system by a similar device process.

ACKNOWLEDGMENTS

We thank G. Eisenstein for helpful discussions, A. Iwai for providing high quality GaN epitaxial wafers, S. Tanisaka for guidance in wafer processing, and T. Mukai and H. Tamaki for sponsoring this project. A preliminary version of these results was given at the CLEO 2022 conference [33]. This work was funded by an Advanced Grant from the European Research Council and by a research grant from Nichia Inc., Japan.

The authors declare that there are no con icts of interest related to this article.

[1] K. J. Vahala, Optical microcavities, Nature **424**, 839 (2003).
[2] W. Bogaerts, P. de Heyn, T. van Vaerenbergh, K. de Vos, S. Kumar Selvaraja, T. Claes, P. Dumon, P. Bienstman, D.

van Thourhout, and R. Baets, Silicon microring resonators, Laser Photonics Rev. **6**, 47 (2012).
[3] H. Lee, T. Chen, J. Li, K. Y. Yang, S. Jeon, O. Painter, and K. J. Vahala, Chemically etched ultrahigh-Q wedge-resonator on a silicon chip, Nat. Photonics **6**, 369 (2012).
[4] D. T. Spencer, J. F. Bauters, M. J. R. Heck, and J. E. Bowers, Integrated waveguide coupled Si_3N_4 resonators in the ultrahigh-Q regime, Optica **1**, 153 (2014).
[5] M. Zhang, C. Wang, R. Cheng, A. Shams-Ansari, and M. Lončar, Monolithic ultra-high-Q lithium niobate microring resonator, Optica **4**, 1536 (2017).
[6] K. Y. Yang, D. Y. Oh, S. H. Lee, Q. F. Yang, X. Yi, B. Shen, H. Wang, and K. Vahala, Bridging ultrahigh-Q devices and photonic circuits, Nat. Photonics **12**, 297 (2018).
[7] S. Honari, S. Haque, and T. Lu, Fabrication of ultra-high Q silica microdisk using chemo-mechanical polishing, Appl. Phys. Lett. **119**, 031107 (2021).
[8] P. Del Haye, A. Schliesser, O. Arcizet, T. Wilken, R. Holzwarth, and T. J. Kippenberg, Optical frequency comb generation from a monolithic microresonator, Nature **450**, 1214 (2007).
[9] D. T. Spencer, *et al.*, An optical-frequency synthesizer using integrated photonics, Nature **557**, 81 (2018).
[10] Z. L. Newman, *et al.*, Architecture for the photonic integration of an optical atomic clock, Optica **6**, 680 (2019).
[11] I. Shomroni, S. Rosenblum, Y. Lovsky, O. Bachler, G. Guendelman, and B. Dayan, All-optical routing of single photons by a one-atom switch controlled by a single photon, Science **345**, 903 (2014).
[12] O. Bechler, A. Borne, S. Rosenblum, G. Guendelman, O. E. Mor, M. Netser, T. Ohana, Z. Aqua, N. Drucker, R. Finkelstein, Y. Lovsky, R. Bruch, D. Gurovich, E. Sha r, and B. Dayan, A passive photon atom qubit swap operation, Nat. Phys. **14**, 996 (2018).
[13] C. T. Santis, S. T. Steger, Y. Vilenchik, A. Vasilyev, and A. Yariv, High-coherence semiconductor lasers based on integral high-Q resonators in hybrid Si/III-V platforms, Proc. Natl. Acad. Sci. U. S. A. **111**, 2879 (2014).
[14] S. Gundavarapu, G. M. Brodnik, M. Puckett, T. Hu man, D. Bose, R. Behunin, J. Wu, T. Qiu, C. Pinho, N. Chauhan, J. Nohava, P. T. Rakich, K. D. Nelson, M. Salit, and D. J. Blumenthal, Sub-hertz fundamental linewidth photonic integrated Brillouin laser, Nat. Photonics **13**, 60 (2019).
[15] M. N. Armenise, V. M. Passaro, F. De Leonardis, and M. Armenise, Modeling and design of a novel miniaturized integrated optical sensor for gyroscope systems, J. Lightwave Technol. **19**, 1476 (2001).
[16] F. Dell Olio, T. Tatoli, C. Ciminelli, and M. N. Armenise, Recent advances in miniaturized optical gyroscopes, J. Eur. Opt. Soc. **9**, 14013 (2014).
[17] Y. H. Lai, M. G. Suh, Y. K. Lu, B. Shen, Q. F. Yang, H. Wang, J. Li, S. H. Lee, K. Y. Yang, and K. Vahala, Earth rotation measured by a chip-scale ring laser gyroscope, Nat. Photonics **14**, 345 (2020).
[18] E. Shumakher and G. Eisenstein, On the noise properties of injection-locked oscillators, IEEE Trans. Microwave Theory Tech. **52**, 1523 (2004).
[19] G. Harari, M. A. Bandres, Y. Lumer, M. C. Rechtsman, Y. D. Chong, M. Khajavikhan, D. N. Christodoulides, and M. Segev, Topological insulator laser: Theory, Science **359**, eaar4003 (2018).
[20] M. A. Bandres, S. Wittek, G. Harari, M. Parto, J. Ren, M. Segev, D. N. Christodoulides, and M. Khajavikhan, Topological insulator laser: Experiments, Science **359**, eaar4005 (2018).
[21] B. Bahari, A. Ndao, F. Valini, A. E. Amili, Y. Fainman, and B. Kant , Nonreciprocal lasing in topological cavities of arbitrary geometries, Science **358**, 636 (2017).
[22] Y. Zeng, U. Chattopadhyay, B. Zhu, B. Qiang, J. Li, Y. Jin, L. Li, A. G. Davies, E. H. Lin eld, B. Zhang, Y. Chong, and Q. J. Wang, Electrically pumped topological laser with valley edge modes, Nature **578**, 246 (2020).
[23] Y. G. Liu, P. Jung, M. Parto, W. E. Hayenga, D. N. Christodoulides, and M. Khajavikhan, in *Novel In-Plane Semiconductor Lasers XIX*, edited by A. A. Belyanin, P. M. Smowton (SPIE, San Francisco, 2020), Vol. 11301, pp. 1130112.
[24] J. H. Choi, W. E. Hayenga, Y. G. Liu, M. Parto, B. Bahari, D. N. Christodoulides, and M. Khajavikhan, Room temperature electrically pumped topological insulator lasers, Nat. Commun. **12**, 3434 (2021).
[25] A. Dikopoltsev, T. H. Harder, E. Lustig, O. A. Egorov, J. Beierlein, A. Wolf, Y. Lumer, M. Emmerling, C. Schneider, S. H ing, M. Segev, and S. Klembt, Topological insulator vertical-cavity laser array, Science **373**, 1514 (2021).
[26] M. Nakamura, A. Yariv, H. W. Yen, S. Somekh, and H. L. Garvin, Optically pumped GaAs surface laser with corrugation feedback, Appl. Phys. Lett. **22**, 515 (1973).
[27] A. Arbabi, S. M. Kamali, E. Arbabi, B. G. Gri n, and L. L. Goddard, Grating integrated single mode microring laser, Opt. Express **23**, 5335 (2015).
[28] S. Klaiman, U. G nther, and N. Moiseyev, Visualization of branch points in PT-symmetric waveguides, Phys. Rev. Lett. **101**, 080402 (2008).
[29] M. A. Miri and A. Al , Exceptional points in optics and photonics, Science **363**, eaar7709 (2019).
[30] J. Wang, M. Feng, R. Zhou, Q. Sun, J. Liu, Y. Huang, Y. Zhou, H. Gao, X. Zheng, M. Ikeda, and H. Yang, GaN-based ultraviolet microdisk laser diode grown on Si, Photonics Res. **7**, B32 (2019).
[31] J. Wang, M. Feng, R. Zhou, Q. Sun, J. Liu, X. Sun, X. Zheng, X. Sheng, and H. Yang, Thermal characterization of electrically injected GaN-based microdisk lasers on Si, Appl. Phys. Express **13**, 074002 (2020).
[32] H. Zhao, M. Feng, J. Liu, X. Sun, T. Tao, Q. Sun, and H. Yang, Unidirectional emission of GaN-on-Si microring laser and its on-chip integration, Nanophotonics **12**, 111 (2023).
[33] S. Tohi, G. Harari, T. Ito, T. Mukai, and M. Segev, in *Conference on Lasers and Electro-Optics* (Optica Publishing Group, San Jose, 2022), p. STu5E.3.